CHAPTER 1

Heat transfer in packed beds

This section covers a discussion of different modes of heat transfer experienced by a pebble in a packed bed. The main modes are conduction to neighbors and convection.

1.1 Single particle modes of heat transfer

The transient energy balance for an irradiated pebble, shown in Fig. 1.1, in a packed bed with flowing interstitial gas is given by Eq. 1.1,

$$\rho V C \frac{\mathrm{d}T}{\mathrm{d}t} = \dot{Q}_g + \dot{Q}_{\text{conduction}} + \dot{Q}_{\text{convection}} + \dot{Q}_{\text{radiation}} \tag{1.1}$$

We begin with the lumped capacitance assumption that internal temperature gradients inside of the solid particle are negligible thus we can neglect diffusion terms in the solid. The validity of that assumption for the ceramic pebbles in fusion reactors will be discussed in detail in §1.1.1. The terms on the right-hand-side of Eq. 1.1 are:

1. Conduction through the stagnant fluid between two point- or non-contacted particles.

2. Conduction through the stagnant fluid between two area-contacted particles.

3. Conduction through the contact area between two area-contacted particles.

4. Conduction through the fluid in void space.

5. Radiation between the surfaces of two particles.

6. Radiation between adjacent voids.

Figure 1.1: Each ceramic pebble in a fusion reactor will experience multiple modes of heat transfer.
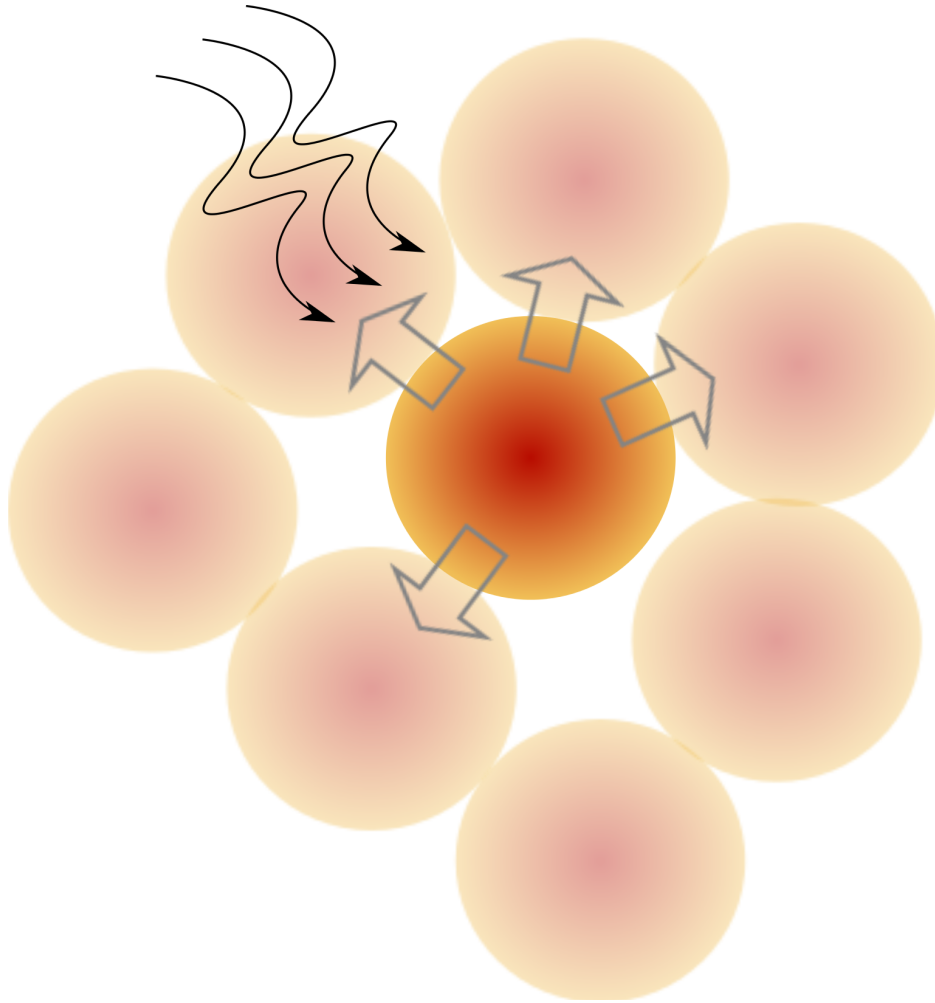
1.1.1 Conduction through the solid

1.2 Solutions to a Sphere in Fluid

We consider a single sphere with volumetric heat generation submerged in and thermally interacting with a fluid. The sphere will be of radius $R = d_p/2$, as shown in Fig. 1.2. The sphere will initially be at a uniform temperature of T_i. The fluid temperature will remain constant at T_f
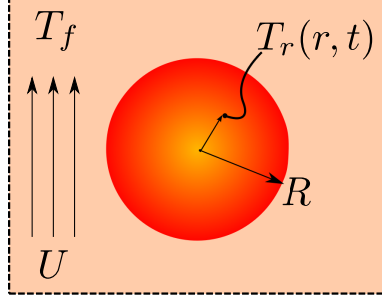
Figure 1.2: CONTROL VOLUME OF A SINGLE SPHERICAL PARTICLE IN A PACKED BED

1.2.1 Lumped Capacitance Solution for Sphere

The lumped capacitance model is assumed for each of the particles in a discrete element method ensemble. Under that assumption, each particle is treated as isothermal and internal heat conduction to the points of contact are neglected. As shown in Fig. 1.2, we will represent a single particle as a sphere initially at temperature T_0, with constant volumetric heat generation, cooling in a fluid with constant heat transfer coefficient. The fluid will remain constant at T_f.

The time response of the sphere's temperature is dictated by the balance of energy to/away from the solid,

$$\rho_r C_r V \frac{dT}{dt} = -hA(T - T_f) + gV \tag{1.2}$$

Eq. 1.2 is solved in dimensionless form with the following nondimensional parameters of temperature and time,

$$\theta = \frac{T(t) - T_f}{T_0 - T_f} \tag{1.3}$$

$$\tau = \frac{t}{b^2/\alpha} \tag{1.4}$$

where b is the radius of the sphere, α is the thermal diffusivity of the sphere, T_0 is the

initial isothermal temperature of the sphere, and T_f is the constant fluid temperature. The resulting temperature distribution is,

$$\theta_{LC} = \left(1 - \frac{G}{3\mathrm{Bi}}\right)\exp(-3\mathrm{Bi}\tau) + \frac{G}{3\mathrm{Bi}} \tag{1.5}$$

where Bi is the familiar Biot number and the dimensionless heat generation term is

$$G = \frac{gb^2}{k(T_0 - T_f)} \tag{1.6}$$

The energy of the sphere, relative to the fluid, in nondimensional terms is

$$E^*(\tau) = \frac{E(\tau)}{E_0} \tag{1.7}$$

where E_0 is the initial energy of the sphere,

$$E_0 = \rho_r C_r V (T_0 - T_f) \tag{1.8}$$

Thus for a sphere with the lumped capacitance model, in nondimensional form, is simply

$$E^*_{LC}(\tau) = \theta_{LC}(\tau) \tag{1.9}$$

The nondimensional energy profile of Eq. 1.9 is plotted over the nondimensional time of $\tau \in [0, 1/\mathrm{Bi}]$ in Fig. 1.3.

Reviewing Eq. 1.5 we see that the speed of decay is dictated by the term in the exponential, 3Bi. Meanwhile, the steady-state value being approached is given by $\frac{G}{3\mathrm{Bi}} = \frac{gb}{h(T_0 - T_f)}$. It is important for this discussion to point out that because both the nondimensional heat generation and Biot number terms contain the solid conductivity, the steady-state value of the lumped capacitance model will not change for varying solid conductivity even if it leads to different Biot numbers. We will return to this point in the next section when we compare the lumped capacitance model to the exact solution when internal conduction of the solid is considered.
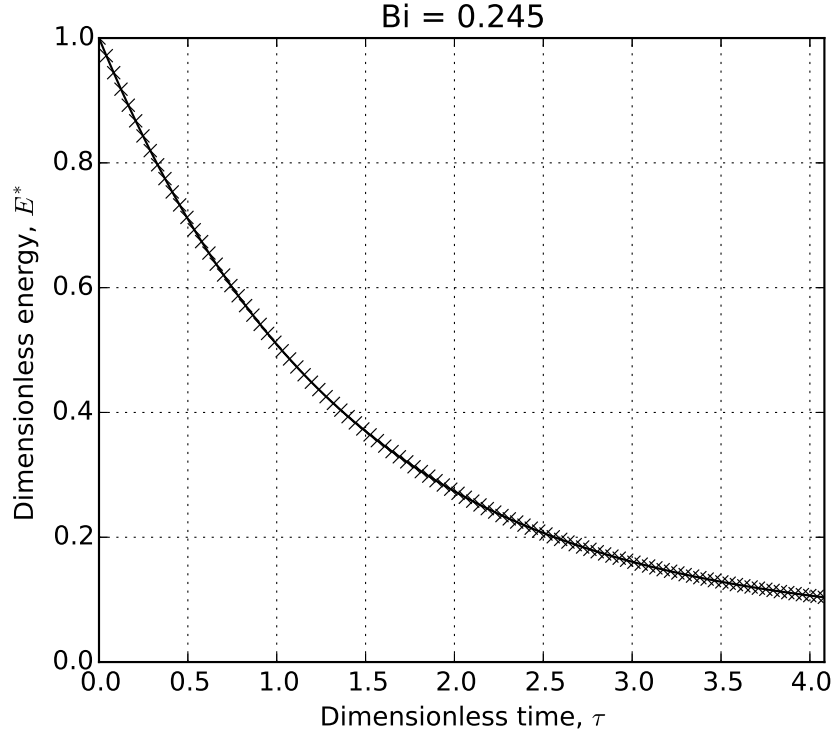
Figure 1.3: Lumped capacitance model: Sphere energy profile decaying from an initial value to a time of 1/Bi

1.2.2 Exact Solution for Sphere

We again analyze the sphere of Fig. 1.2 but now will account for internal temperature gradients inside the sphere. The details of the analytic solution for a sphere with heat generation interacting with a fluid is given in Appendix .1. We again solve in terms of the nondimensional temperature and time introduced in § 1.2.1 as well as a nondimensional radius,

$$\theta = \frac{\mathbb{T}}{\mathbb{T}_0}$$

$$\rho = \frac{r}{b}$$

$$\tau = \frac{t}{b^2/\alpha}$$

5

The energy conservation equation for the sphere with internal temperature gradient, in nondimensional form θ_{TG}, is

$$\frac{1}{\rho}\frac{\partial^2}{\partial\rho^2}(\rho\theta_{TG}) + G = \frac{\partial\theta_{TG}}{\partial\tau} \tag{1.10}$$

With the initial condition and boundary conditions outlined in Appendix .1, the nondimensional temperature distribution inside the sphere is

$$\theta_{TG}(\rho,\tau) = \left(\frac{G}{6} + \frac{G}{3\text{Bi}} - \rho^2\right) + \sum_{n=1}^{\infty}\exp(-\zeta^2\tau)\frac{\sin(\zeta_n\rho)}{\rho}\frac{Z(\zeta_n)}{N(\zeta_n)} \tag{1.11}$$

where ζ_n are the eigenvalues of the problem and the functions of $zeta_n$ (Z,N,C) are given in Appendix 1.2.2.

The accompanying nondimensional energy of the sphere is,

$$E^*_{TG}(\tau) = \left(\frac{G}{15} + \frac{G}{3\text{Bi}}\right) + 3\sum_{n=1}^{\infty}\exp(-\zeta^2\tau)\frac{Z(\zeta_n)}{N(\zeta_n)}C_n(\zeta_n) \tag{1.12}$$

We now compare the exact solution from Eq. 1.12 to the solution of energy given by the lumped capacitance model of Eq. 1.9. The two profiles are given in Fig. 1.4.

For the value of Biot number here, Bi < 0.5, the profile of the analytic solution of the sphere is well-captured by the lumped capacitance model. The maximum relative error over the time span, as defined by

$$\text{error} = \frac{\left|E^*_{TG}(\tau) - E^*_{LC}(\tau)\right|}{E^*_{TG}(\tau)} \tag{1.13}$$

is always less than 10%.

We consider now the same size sphere but with the Biot number increased by an order by: a) a conductivity of $k = k_r/10$ and b) a heat transfer coefficient of $h = 10h_f$. The two physical changes to the system result in the same Biot number but as we can see in Fig. 1.5, there are drastic changes in the results.
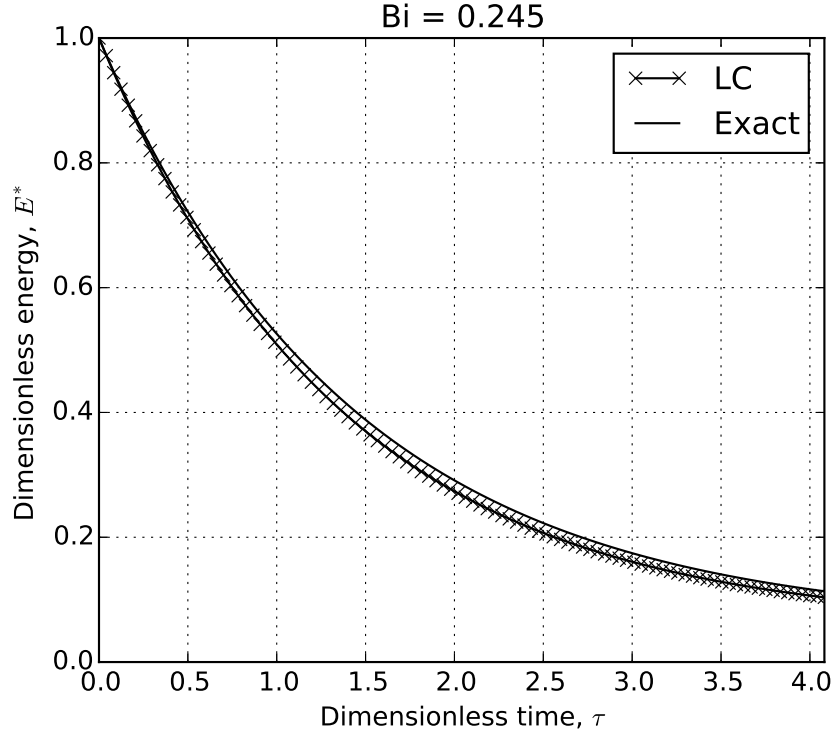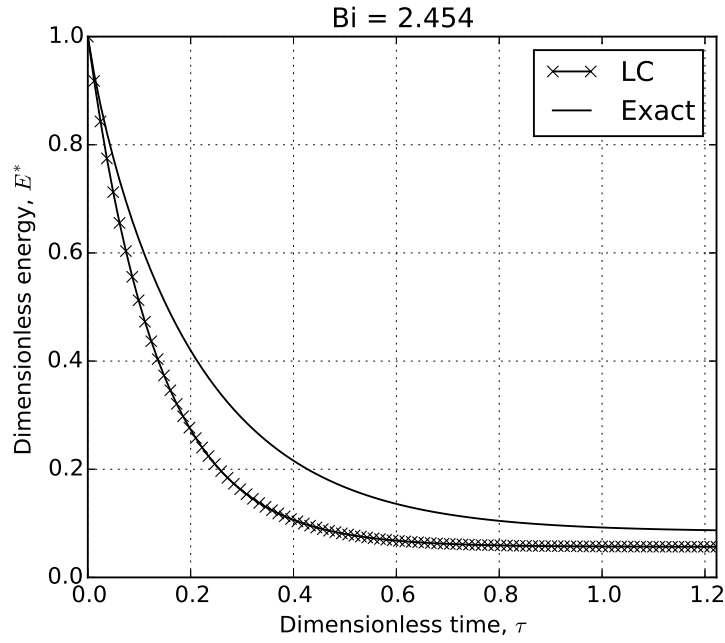
Figure 1.4: Analytic and lumped capacitance models: Sphere energy profile decaying from an initial value to a time of 1/Bi

Seen in Fig. 1.5a, the lumped capacitance solution both over-predicts the speed at which the sphere reaches a thermal steady-state as well as the value of the steady-state. Comparatively, in Fig. 1.5b, for the same Biot number the lumped capacitance solution again over-predicts the speed to thermal steady-state by the same rate but is relatively accurate for the steady-state value itself.
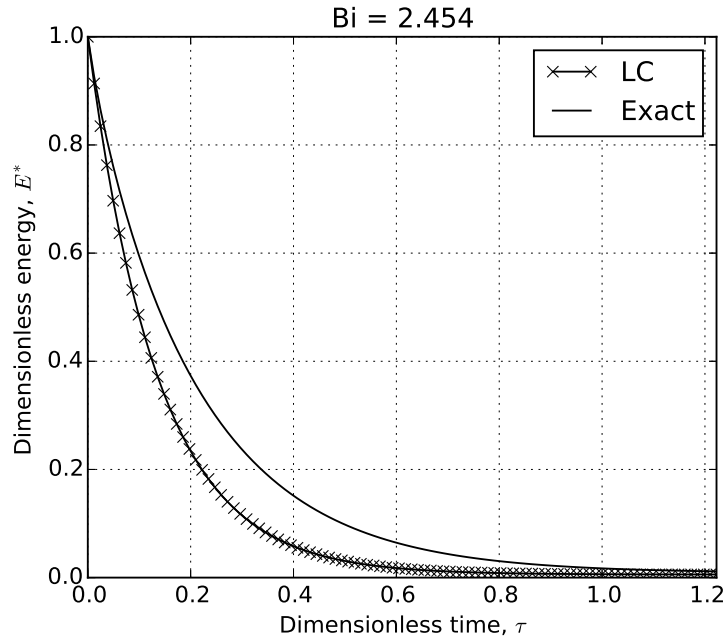
To first address the source of error on the steady-state value, we view the steady-state terms of the two solutions. From Eq. 1.12, we write the steady-state term of the exact solution as

$$E_{TG,ss}^* = \frac{G}{15} + \frac{G}{3\text{Bi}} \tag{1.14}$$

Comparatively, we write the steady-state term of the lumped capacitance solution from

(a) The Biot number increased from a decrease in the solid conductivity.

(b) The Biot number increased from an increase in the heat transfer coefficient.

Figure 1.5: Analytic and lumped capacitance models: Sphere energy profile decaying from an initial value to a time of $3/Bi$. The same Biot number produces different results for the exact solution of a sphere with heat generation.

8

§ 1.2.1 as,

$$E^*_{LG,ss} = \frac{G}{3\mathrm{Bi}} \tag{1.15}$$

We clearly see that the two steady-state values differ by the contribution of $\frac{G}{15}$ on the exact solution. This term does not appear in the lumped capacitance solution because it does not account for the temperature difference through the sphere. The nondimensional heat generation term is given in Eq. 1.6; it is importantly a function of thermal conductivity but not the heat transfer coefficient. This explains the difference between steady-state values in Fig. 1.5.

To address the inaccuracies in the time-dependent response of the lumped capacitance method with large Biot number, we will make use of the so-called Jeffreson Correction described by Van Lew[?] and Xu, et al.[?] In their work, they considered a heated heat transfer fluid interacting with a low conductivity thermal storage material. The solar thermal storage systems often had large Biot numbers but they could continue to apply the lumped capacitance model by accounting for the large Biot number with the Jeffreson Correction.[?] The details of the Jeffreson correction as applied to a system with volumetric heat generation will be discussed next.

1.2.3 Jeffreson Correction Solution

In Fig. 1.5, the lumped capacitance model predicted a much faster decay to steady-state than the exact solution. Jeffreson summarized a correction to the lumped capacitance model via a reduction in the heat transfer coefficient as a function of the Biot number. The smaller heat transfer coefficient effectively slowed the decay to steady-state as predicted by the lumped capacitance method. The correlation to correct the heat transfer coefficient due to solids with large Biot number is given by Jeffreson.[?] The Jeffreson correction for a sphere is,

$$h_p = \frac{h}{1 + \mathrm{Bi}/5} \tag{1.16}$$

where h_p is the modified heat transfer coefficient of the particle with an internal temperature gradient. An increase in the Biot Number (or increase of thermal gradient inside the solid) results in a decrease in the heat transfer coefficient h_p. A modified Biot number can then also be written as

$$\mathrm{Bi}_p = \frac{h_p d}{k_r} = \frac{\mathrm{Bi}}{1 + \mathrm{Bi}/5} \tag{1.17}$$

Applying the Jeffreson Correction to Eq. 1.5,

$$\theta_{JC} = \left(1 - \frac{G}{3\mathrm{Bi}_p}\right) \exp\left(-3\mathrm{Bi}_p \tau\right) + \frac{G}{3\mathrm{Bi}_p} \tag{1.18}$$

and thereby Eq. 1.9 gives

$$E_{JC}^*(\tau) = \theta_{JC}(\tau) \tag{1.19}$$

We then plot the energy profiles from the lumped capacitance model (LC), the Jeffreson correction (JC), and the exact solution together in Fig. 1.6
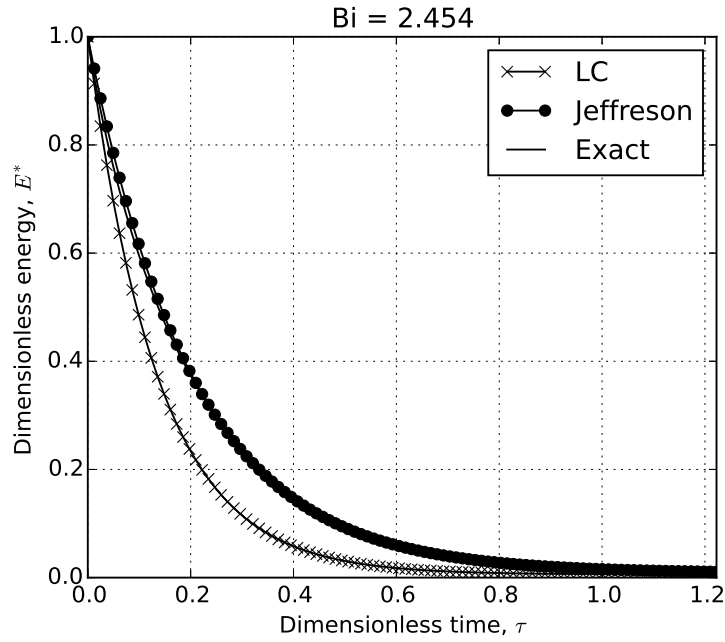
The Jeffreson correction to the lumped capacitance method allows the simple model to capture the proper transient as well as steady-state values for this sphere with a moderately sized Biot number. To look more closely, we view the instantaneous error (see Eq. 1.13) in Fig. 1.7.

For the value of $\mathrm{Bi} > 1$ due to either low conductivity (Fig. 1.7a) or high heat transfer coefficient (Fig. 1.7b), the error in the Jeffreson correction is always under 10%; often closer to only 1%. This is in opposition to the standard lumped capacitance method which has 50-80% error for both transient and steady-state values.

The lumped capacitance method allows researchers to simplify transient, conjugate heat transfer problems with an isothermal solid. In the discrete element method, the assumption of isothermal solid is innate in the framework of the method. With the implementation of the Jeffreson correction in the discrete element method, we have confidence in the fidelity
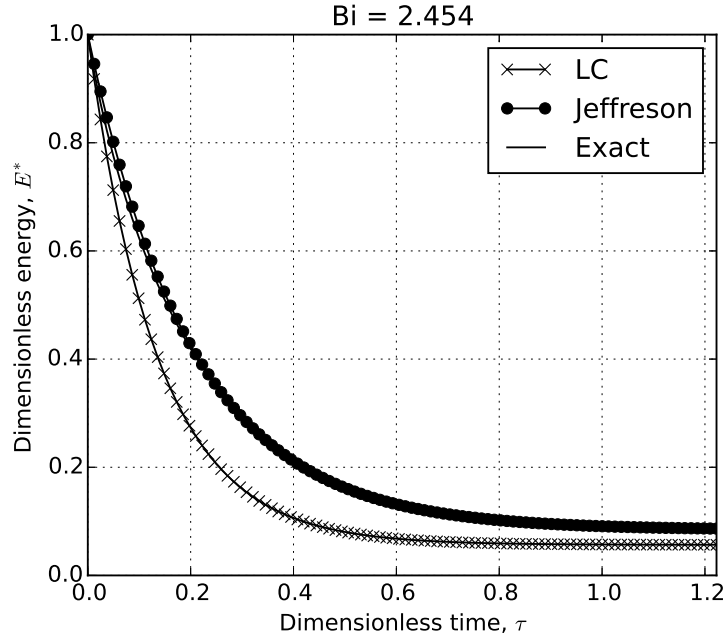
(a) The Biot number increased from a decrease in the solid conductivity.

(b) The Biot number increased from an increase in the heat transfer coefficient.

Figure 1.6: Error of lumped capacitance and reduced error of the model with Jeffreson correction for moderate Biot number.
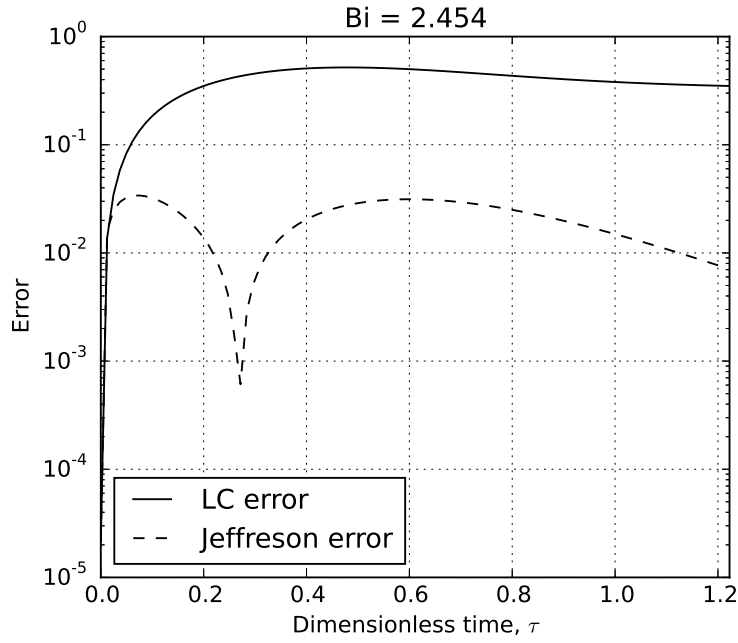
(a) The Biot number increased from a decrease in the solid conductivity.
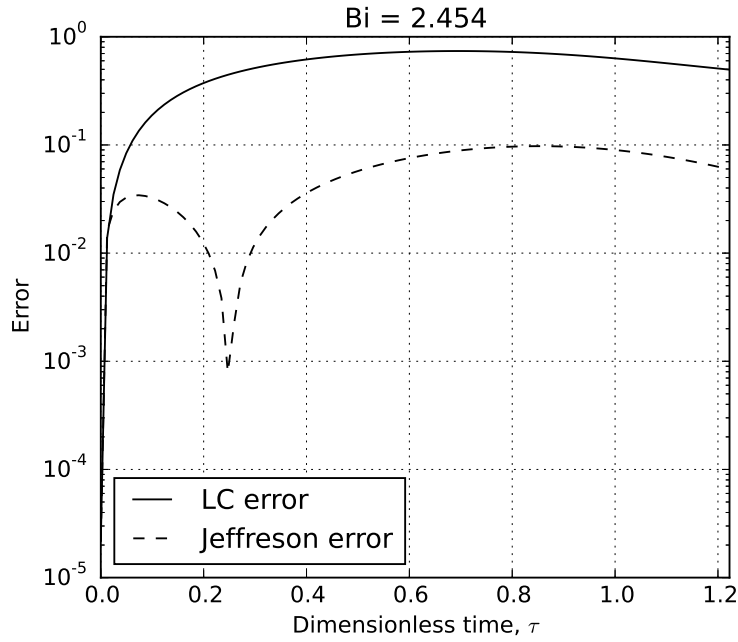
(b) The Biot number increased from an increase in the heat transfer coefficient.

Figure 1.7: Analytic, lumped capacitance model, and LC model with Jeffreson correction: Jeffreson correction corrects for transient and steady-state errors of lumped capacitance.

of the heat transfer in for moderately sized Biot numbers. The Jeffreson correction will be implemented into the DEM computations via Eq. 1.17.

1.3   Inter-particle heat conduction

Handling the heat transfer between contacting particles has been investigated extensively by researchers in a number of fields.[?,?,?,?,?,?]

In the Hertz analysis we walked through in §**??**, we found the contact radius of two elastic spheres in Eq. **??** as a function of the contact pressure. We rewrite the radius in terms of the compression force acting on the bodies,

$$a = \left(\frac{3}{4}\frac{R^*}{E^*}\right)^{1/3} F^{1/3} \tag{1.20}$$

where $\frac{1}{E^*} = \frac{1-\nu_1^2}{E_1} + \frac{1-\nu_2^2}{E_2}$ and $\frac{1}{R^*} = \frac{1}{R_1} + \frac{1}{R_2}$ as before.

Batchelor and O'Brien[?] made the brilliant observation that the temperature fields in the near-region of contacting spheres are analogous to the velocity potential of the potential flow of a fluid passing from from one reservoir to another through a circular hole in a planar wall. With the analogy, they could make use of the fluid flow solution to write the total flux across the circle of contact,

$$Q_{ij} = H_{ij}(T_i - T_j) \tag{1.21}$$

with the heat conductance,

$$H_{ij} = 2k_s a = 2k_s \left(\frac{3}{4}\frac{R^*}{E^*}\right)^{1/3} F^{1/3} \tag{1.22}$$

governing the time rate of energy transferred per temperature difference between particles, T_i and T_j, respectively. This approach, laid out by Batchelor and O'Brien, is valid when the thermal conductivity ratio of solid and fluid is well above unity and the contact area is small relative to the particle. The condition is expressed as,

$$\frac{k_s}{k_f}\frac{a}{R^*} = \lambda \gg 1 \tag{1.23}$$

The model, being derived from Hertz theory, also carries with it many of the assumptions and limitations inherent with that theory. The assumptions are discussed in detail in §**??**.

Recently, Cheng, et al.[?] proposed a slightly modified variant of the conductance given by Batchelor and O'Brien. In their model, they allow for contacting materials of different thermal conductivity. Therefore they have,

$$H_{ij} = 2k^*a = 2k^* \left(\frac{3}{4}\frac{R^*}{E^*}\right)^{1/3} F^{1/3} \tag{1.24}$$

where $\frac{1}{k^*} = \frac{1}{k_i} + \frac{1}{k_j}$. As well as being a more general, flexible formulation, the models analyzed by Cheng, et al.[?] are in good agreement with experiments and will be used in this study.

1.3.0.1 Large Biot number

Considering now material and geometric properties relevant to our ceramic pebble beds, we will see that we may need to consider the effects of a larger Bi for our pebbles. The helium purge gas moving through the packed beds is not specifically intended to act as a heat transfer agent and moves along at a creeping flow rate. For a first approximation we will therefore assume as a lower limit the Nusselt number is Nu = 2 (the value for a sphere in quiescent fluid). From the requirement that Bi $\ll$ 1, we have

$$2\frac{k_f}{k_s} \ll 1 \tag{1.25}$$

The conductivity of helium over the temperature range of 300 to 800 °C is approximately $0.3\,\mathrm{W/m-K}$. The solid conductivity of $\mathrm{Li_2TiO_3}$ and $\mathrm{Li_4SiO_4}$ are approximately $2\,\mathrm{W/m-K}$. Because of the low conductivity of our solid, the Biot assumption is barely valid, $0.3 < 1$.

1.4 Nusselt number for spheres in packed beds

1.4.1 Convection by interstitial gas

Engineers have paid considerable attention to the calculation of convective heat transfer in packed beds. Correlations for determining the Nusselt number of a sphere in dilute and dense packings over a range of Reynolds and Prandtl number are available. We will cover the detail of many of these correlations in §**??**. The methods all come down to calculating Nusselt number to find the heat transfer coefficient and then computing the rate of heat transfer from convection as

$$\dot{Q}_{\text{convection}} = -hA(T_s - T_f) \tag{1.26}$$

where T_s is the temperature of the solid with surface area, A, and T_f is the local bulk temperature of the passing fluid. The negative sign is to maintain convention that energy transfer into the solid is positive.

1.4.2 Radiative transfer with neighboring particles

The temperatures expected in the solid breeder are high enough that we can not a priori neglect radiation. The radiation exchange between contacting neighbors in a packed bed becomes extremely complex due to the local and semi-local nature of radiation. A standard approach to treat radiation exchange between surfaces is to consider the view factor between them. In a dense, randomly packed bed of spheres the computation of view factors between pebbles can be done via a method such as that proposed Feng and Han.[?] Ideally, we could show this mode of heat transport is negligible compared to the others already discussed.

In ceramic breeder designs, the tritium breeding volume is rarely more than 2cm wide with pebbles that are, generally, 1mm in diameter. The maximum expected temperature in the breeding zone is about 1000K, roughly at the centerline of the 2cm width. The walls of the coolant must be held below the operable steel temperature of roughly 700K. This

works out to a 300K differences spanning 10 pebble diameters. From this we can make a first-order approximation of 30K difference between neighboring pebbles. At the elevated temperatures, an estimate for the radiation exchange between two pebbles (allowing them to act as black bodies for this approximation) is

$$\dot{Q}_{\text{radiation}} = \sigma A \left(T_{\max}^4 - (T_{\max} - 30)^4 \right) \approx 0.022 \text{W} \tag{1.27}$$

which is the highest amount of radiation exchange we might expect between pebbles.

.1 Sphere with heat generation

We solve for the temperature distribution inside a single sphere of constant thermal conductivity with constant heat generation with a convective heat transfer boundary condition. To simplify to homogeneous boundary conditions, the temperature we solve for will be in reference to the fluid temperature, $\mathbb{T} = T - T_f$.

The energy equation in spherical coordinates with axial symmetry is,

$$\frac{1}{r}\frac{\partial^2}{\partial r^2}(r\mathbb{T}) + \frac{g}{k} = \frac{1}{\alpha}\frac{\partial \mathbb{T}}{\partial t} \tag{.28}$$

which is subject to the boundary conditions of a constant heat transfer coefficient at the surface, h,

$$\left[\frac{\partial \mathbb{T}}{\partial r} + \frac{h}{k}\mathbb{T} \right]_{r=b} = 0 \tag{.29}$$

and an axisymmetry at the center,

$$\left[\frac{\partial \mathbb{T}}{\partial r} \right]_{r=0} = 0 \tag{.30}$$

The sphere will be at an isothermal initial temperature,

16

$$\mathbb{T}(r,0) = \mathbb{T}_0 \tag{.31}$$

.1.1 Transformations

We first transform the system into the nondimensional forms as defined in § 1.1.1,

$$\theta = \frac{\mathbb{T}}{\mathbb{T}_0}$$

$$\rho = \frac{r}{b}$$

$$\tau = \frac{t}{b^2/\alpha}$$

The energy equation is then,

$$\frac{1}{\rho}\frac{\partial^2}{\partial\rho^2}(\rho\theta) + G = \frac{\partial\theta}{\partial\tau} \tag{.32}$$

where $G = \frac{gb^2}{k\mathbb{T}_0}$

The next transformation will be to introduce $U(\rho,\tau) = \rho\theta(\rho,\tau)$ as a transformation variable to simplify the differential equation of energy conservation. In the new variable formulation, the energy equation is,

$$\frac{\partial^2 U}{\partial\rho^2} + G\rho = \frac{\partial U}{\partial\tau} \tag{.33}$$

The boundary conditions are likewise transformed into,

$$\left[\frac{\partial U}{\partial\rho} + (\mathrm{Bi} - 1)\,U\right]_{\rho=1} = 0 \tag{.34}$$

and

$$U\big|_{\rho=0} = 0 \tag{.35}$$

with initial condition

$$U(\rho, 0) = U_0 = \theta_0 r^* = r^* \tag{.36}$$

.1.2 Solution

Because of the non-homegeneous form of the energy equation (due to the heat generation term), we will solve Eq. .33 by breaking it up into two simpler problems,

1. A non-homogeneous, steady-state problem defined by $U_{ss}(r)$

2. A homogeneous, time-dependent problem defined by $U_h(r, t)$

The steady-state distribution U_{ss} is found from the solution of

$$\frac{\partial^2 U_{ss}}{\partial \rho^2} + G\rho = 0 \tag{.37}$$

subject to the same boundary condition given by Eqs. .34,.35. Separation and integration gives.

$$U_{ss} = -\frac{G}{6}\rho^3 + C_1\rho + C_2 \tag{.38}$$

Applying Eq. .35 directly gives $C_2 = 0$ and, with some algebra Eq. .34 gives,

$$C_1 = \left(\frac{G}{6} + \frac{G}{3\mathrm{Bi}}\right)$$

valid for $\mathrm{Bi} > 0$. Thus the steady-state distribution of our transformed variable is

$$U_{ss} = \left(\frac{G}{6} + \frac{G}{3\mathrm{Bi}} - \rho^2\right)\rho \tag{.39}$$

The next step is to find the homogeneous solution of

18

$$\frac{\partial^2 U_h}{\partial \rho^2} = \frac{\partial U_h}{\partial \tau} \qquad (.40)$$

Again, subject to Eqs. .34,.35, but now with a modified initial condition of

$$
\begin{aligned}
U_{h,0} &= U_0 - U_{ss} \\
&= \left[1 - \left(\frac{G}{6} + \frac{G}{3\mathrm{Bi}} - \rho^2 \right) \right] \rho
\end{aligned} \qquad (.41)
$$

This is a standard homogeneous partial differntial equation. The solution is of the form

$$U_h = R(\rho)\Gamma(\tau) \qquad (.42)$$

The solution for Γ is given as

$$\Gamma = \exp(-\zeta^2 \tau) \qquad (.43)$$

The space-variable function $R(\zeta, \rho)$ satisfies the following eigenvalue problem:

$$\frac{\mathrm{d}^2 R}{\mathrm{d}\rho^2} + \zeta^2 R = 0 \qquad (.44)$$

subject to

$$R_{\rho=0} = 0 \qquad (.45)$$

and

$$\left[\frac{\mathrm{d}R}{\mathrm{d}\rho} + (\mathrm{Bi} - 1)R \right]_{\rho=1} = 0 \qquad (.46)$$

This eigenvalue problem is a special case of the Sturm-Liouville problem. The solution for U_h can be constructed from known eigenvalue solutions,

19

$$U_h(\rho, \tau) = \sum_{n=1}^{\infty} c_n R(\zeta_n, \rho) \exp(-\zeta^2 \tau) \tag{.47}$$

Application of the initial condition gives,

$$F(\rho) = \sum_{n=1}^{\infty} c_n R(\zeta_n, \rho) \tag{.48}$$

where $F(\rho)$ is the initial condition defined from Eq .36,

$$F(\rho) = \left[1 - \frac{G}{6}\left(1 + \frac{2}{\text{Bi}} - \rho^2\right)\right]\rho \tag{.49}$$

The coefficients of c_n can be determined by applying the operator $\int_0^1 R(\zeta_n, \rho)\, d\rho$ and utilizing the orthogonality property of eigenfunctions. The coefficients are found in the form

$$c_n = \frac{1}{N(\zeta_n)} \int_0^1 R(\zeta_n, \rho') F(\rho')\, d\rho' \tag{.50}$$

The norm, N is a function of the eigenvalues,

$$N(\zeta_n) = \int_0^1 [R(\zeta_n, \rho)]^2\, d\rho \tag{.51}$$

The eigenfunctions for Eq. .44 are

$$R(\zeta_n, \rho) = \sin(\zeta_n \rho) \tag{.52}$$

where the eigenvalues are the root of the following transcendental equation,

$$\zeta_n \cot(\zeta_n) = -H \tag{.53}$$

the roots of which will be found numerically. The normalization integral is then solved as

$$\frac{1}{N(\zeta_n)} = 2\frac{\zeta_n^2 + H^2}{\zeta_n^2 + H^2 + H} \tag{.54}$$

where $H = (\text{Bi} - 1)$.

We substitute the coefficients of Eq. .50, they can be substituted back into Eq. .47 and we have a solution for the homogeneous, transient distribution,

$$U_h(\rho, \tau) = \sum_{n=1}^{\infty} \exp(-\zeta^2 \tau)\frac{R(\zeta_n, \rho)}{N(\zeta_n)} \int_0^1 R(\zeta_n, \rho')F(\rho')\,\mathrm{d}\rho' \tag{.55}$$

In order to explicitly express the solution, we will first set the integral equal to a function $Z(\zeta_n)$ and evaluate as,

$$
\begin{aligned}
Z(\zeta_n) &= \int_0^1 R(\zeta_n, \rho')F(\rho')\,\mathrm{d}\rho' \\
&= \int_0^1 \sin(\zeta_n \rho')\left[1 - \left(\frac{G}{6} + \frac{G}{3\text{Bi}} - \rho'^2\right)\right]\rho'\,\mathrm{d}\rho' \\
&= \left[1 - \left(\frac{G}{6} + \frac{G}{3\text{Bi}}\right)\right]\int_0^1 \sin(\zeta_n \rho')\rho'\,\mathrm{d}\rho' + \frac{G}{6}\int_0^1 \sin(\zeta_n \rho')\rho'^3\,\mathrm{d}\rho' \tag{.56}
\end{aligned}
$$

The two unique integrals are evaluated as

$$
\begin{aligned}
C_n &= \int_0^1 \sin(\zeta_n \rho')\rho'\,\mathrm{d}\rho' = \frac{\sin\zeta_n - \zeta_n\cos\zeta_n}{\zeta_n^2} \\
K_n &= \int_0^1 \sin(\zeta_n \rho')\rho'^3\,\mathrm{d}\rho' = \frac{3(\zeta_n^2 - 2)\sin\zeta_n - \zeta_n(\zeta_n^2 - 6)\cos\zeta_n}{\zeta_n^4}
\end{aligned}
$$

Thus our Z function is

$$Z(\zeta_n) = \left[1 - \left(\frac{G}{6} + \frac{G}{3\text{Bi}}\right)\right]C_n + \frac{G}{6}K_n \tag{.57}$$

The homogeneous solution is then written in a compact form as,

$$U_h(\rho, \tau) = \sum_{n=1}^{\infty} \exp(-\zeta^2 \tau)\sin(\zeta_n \rho)\frac{Z(\zeta_n)}{N(\zeta_n)} \tag{.58}$$

The complete solution is then a superposition of Eq. .39 and Eq. .58,

$$U(\rho, \tau) = \left(\frac{G}{6} + \frac{G}{3\mathrm{Bi}} - \rho^2 \right) \rho + \sum_{n=1}^{\infty} \exp(-\zeta^2 \tau) \sin(\zeta_n \rho) \frac{Z(\zeta_n)}{N(\zeta_n)} \tag{.59}$$

We now transform back to our dimensionless temperature,

$$\theta(\rho, \tau) = \left(\frac{G}{6} + \frac{G}{3\mathrm{Bi}} - \rho^2 \right) + \sum_{n=1}^{\infty} \exp(-\zeta^2 \tau) \frac{\sin(\zeta_n \rho)}{\rho} \frac{Z(\zeta_n)}{N(\zeta_n)} \tag{.60}$$

.1.3   Energy

We will want to compare the solution of Eq. .60 to that of a sphere with the lumped capacitance assumption. To facilitate comparison, we look to a measure of the energy of the sphere (with radial dependence removed via integration of Eq. .60). The energy will be nondimensionalized as,

$$E^*(\tau) = \frac{E(\tau)}{E_0} \tag{.61}$$

where E_0 is the initial energy of the sphere,

$$E_0 = \rho_r C_r V \mathbb{T}_0 \tag{.62}$$

Thus the nondimensional energy of the sphere at a given time, τ is

$$E^*(\tau) = \int \frac{\rho_r C_r \mathbb{T}(\rho, \tau) \mathrm{d}V}{\rho_r C_r V \mathbb{T}_0}$$
$$E^*(\tau) = \frac{1}{V} \int \theta(\rho, \tau) \, \mathrm{d}V \tag{.63}$$

For a circle in spherical coordinates:

$$\mathrm{d}V = r^2 \sin(\phi) \mathrm{d}r \mathrm{d}\phi \mathrm{d}\theta \tag{.64}$$

22

For our sphere, this becomes:

$$\mathrm{d}V = 4\pi b^3 \rho^2 \mathrm{d}\rho = 3V \rho^2 \mathrm{d}\rho \tag{.65}$$

The integral for dimensionless energy of our sphere is then,

$$E = 3 \int_0^1 \left[\frac{G}{6} \left(1 + \frac{2}{\mathrm{Bi}} - \rho^2 \right) + \sum_{n=1}^{\infty} \exp(-\zeta^2 \tau) \frac{\sin(\zeta_n \rho)}{\rho} \frac{Z(\zeta_n)}{N(\zeta_n)} \right] \rho^2 \, \mathrm{d}\rho \tag{.66}$$

This ultimately reduces to,

$$E^* = \left(\frac{G}{15} + \frac{G}{3\mathrm{Bi}} \right) + 3 \sum_{n=1}^{\infty} \exp(-\zeta^2 \tau) \frac{Z(\zeta_n)}{N(\zeta_n)} C_n(\zeta_n) \tag{.67}$$